Separation Science and Technology
Publication details, including instructions for authors and subscription information:
http://www.informaworld.com/smpp/title~content=t713708471

Effect of Temperature on Chiral Separation of Ketamine Enantiomers by High-Performance Liquid Chromatography

Ivanildo José da Silva Junior[a]; Marco Antônio Garcia dos Santos[a]; Vinícius de Veredas[a]; Cesar Costapinto Santana[a]
[a] Laboratory of Bioseparations, Department of Biotechnology Processes, School of Chemical Engineering, State University of Campinas, UNICAMP, Campinas, SP, Brazil

To cite this Article Junior, Ivanildo José da Silva , Santos, Marco Antônio Garcia dos , de Veredas, Vinícius and Santana, Cesar Costapinto(2005) 'Effect of Temperature on Chiral Separation of Ketamine Enantiomers by High-Performance Liquid Chromatography', Separation Science and Technology, 40: 13, 2593 — 2611
To link to this Article: DOI: 10.1080/01496390500283258
URL: http://dx.doi.org/10.1080/01496390500283258

Separation Science and Technology, 40: 2593–2611, 2005

ISSN 0149-6395 print/1520-5754 online
DOI: 10.1080/01496390500283258

Effect of Temperature on Chiral Separation of Ketamine Enantiomers by High-Performance Liquid Chromatography

Ivanildo José da Silva Junior, Marco Antônio Garcia dos Santos, Vinícius de Veredas and Cesar Costapinto Santana

Laboratory of Bioseparations, Department of Biotechnology Processes, School of Chemical Engineering, State University of Campinas, UNICAMP, Campinas, SP, Brazil

Abstract: A semipreparative column packed with microcrystalline cellulose triacetate (MCTA) was used to separate ketamine enantiomers by high-performance liquid chromatography (HPLC). The effect of temperature on the kinetics of mass transfer and equilibrium constants were evaluated by the moment analysis at 303, 313, and 323 K. Total porosity, bed porosity, and equilibrium constants were measured by the first moment. Pore diffusion and axial dispersion coefficients were evaluated by the second moment. It was observed that band broadening decreased with increasing temperature. The equilibrium constants were found to be greater than unity and decreasing with increasing temperature. The pore diffusion coefficients increased with increasing temperature and the main contribution to the band broadening was attributed to low mass transfer kinetics. The pore diffusion coefficients controlled the mass-transfer process in MCTA column. These results may be used to the determination of operating conditions and computational simulation of a chromatographic separation in simulated moving bed unity.

Keywords: Liquid chromatography, chiral separation, adsorption, mass transfer, equilibrium

Received 7 April 2005, Accepted 15 June 2005

Address correspondence to Professor Dr. Cesar Costapinto Santana, Laboratory of Bioseparations, Department of Biotechnology Processes, School of Chemical Engineering, State University of Campinas, UNICAMP, P.O. Box: 6066, 13083-970, Campinas, SP, Brazil. E-mail: santana@feq.unicamp.br

INTRODUCTION

Preparative liquid chromatography becomes more and more an important separation process for the isolation and purification of pharmaceuticals, biomolecules, and other added products. Higher requirements on the product purity, growing importance of enantioseparations, and improved availability of highly selective stationary phases promote this trend. However, chromatographic techniques are expensive and require in an industrial scale a careful optimization of the operating conditions with respect to production rates, recoveries, and separation costs. The most common technique used in preparative chromatography is still isocratic batch elution, however, more sophisticated concepts as recycling, gradient elution, displacement, or the simulated moving bed (SMB) process are increasingly applied to enhance the productivity and yields. In general, it is not an easy task to design and optimize these processes and to perform a quantitative comparison between rivaling concepts (1). Theoretical modeling and simulation can be used to predict the performance of these systems and to provide a helpful tool for design of scaled-up units and optimization of their operating conditions. The reliability of simulation has to be built on accurate adsorption characteristics, including the equilibrium and kinetic model parameters (2).

The behavior of a chromatographic system is governed by three basic phenomena (3): *i*) the adsorption thermodynamics, described by equilibrium isotherms which give the composition in the stationary phase vs. the composition in the mobile phase when equilibrium is reached, at given temperature; *ii*) the column hydrodynamics, i.e., the properties of the flow through the porous medium; *iii*) the mass-transfer kinetics. These parameters are very important in the modeling and simulation of chromatographic processes as well as for the design of the operating conditions of an SMB unit.

In chromatography, the position of elution peak in chromatography depend essentially on the thermodynamics of phase equilibrium, especially at high concentrations, when the asymmetry of the elution profile is strongly and foremost influenced by the curvature of the nonlinear equilibrium isotherm (4). At low concentrations (dilute conditions) usually used in analytical chromatography the isotherms are linear. In large-scale applications of chromatography more concentrated solutions are usually separated and non-linear solutions are usually required. However, linear chromatographic solutions are very useful for the insight they give on the importance of mass transfer and dispersion (5). Under dilute conditions a small pulse is dispersed by mass-transfer effects as it migrates through a column. Axial dispersion and the mass-transfer processes provide the sources of band broadening in linear chromatography (6).

Microcrystalline cellulose triacetate (MCTA) is one of the first chiral stationary phases (CSPs) used for preparative chromatographic enantioseparations (7) (Fig. 1). MCTA is produced by the heterogeneous acetylation of microcrystalline cellulose (8) and has been widely employed as chiral discriminator in liquid chromatography (9). The ability of MCTA for chiral

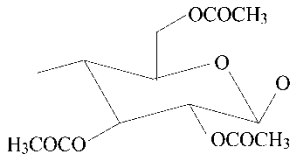

Figure 1. Chemical structure of MCTA.

recognition originates from the crystalline nature of native cellulose (10). Despite the large number of chiral separations described by MCTA, the mechanisms of interaction that control chiral separations are not yet well understood with several hypotheses being offered. All evidence seems to point to an inclusion mechanism for enantioselectivity in MCTA by shape-selective adsorption into chiral cavities in the polymer network (11, 12). Pais et al. (13) reported that adsorption in MCTA is more influenced by steric effects than by the chemical nature of the interaction between the chiral species and the stationary phase substituents.

The large band broadening usually observed in chromatographic separations results in reduced efficiency and limits the use of MCTA for analytical purposes. This phenomenon was carefully studied with respect to the adsorbed solute capacity factor and structure, mobile phase flow-rate, adsorbent saturation, eluent composition, temperature, and pressure (14–16). It was concluded that in columns packed with MCTA the greatest contribution to the plate height arises from slow mass transfer in the packed bed. This is attributed to a slow transport process at narrow adsorption sites: slow diffusion and orientation at narrow sites, in narrow channels, or in cavity-like structures (15, 16).

Ketamine (Fig. 2) is commercially available as a racemate (*S*- and *R*-ketamine). It is a dissociative anesthetic agent that has been widely used in clinical practice (17, 18). *S*-ketamine is four times more potent in analgesia than *R*-ketamine (17). In addition, it does not induce the undesirable psychological reactions, such as vivid dreams and hallucinations in human where these collateral effects are attributed to *R*-ketamine (19).

Santos et al. (20) published a paper describing the separation of ketamine enantiomers in MCTA using a SMB unity. More recently, Silva Jr. et al. (21) published a paper describing the chromatographic separation parameters of ketamine in MCTA at 298 K. The kinetic data were obtained by pulse

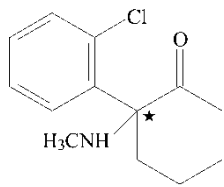

Figure 2. Chemical structure of ketamine. The symbol (★) denotes the chiral center.

experiments under linear conditions and the nonlinear adsorption isotherms were so determined by frontal analysis experiments. However, any systematic study regarding the effect of the temperature on the separation of the ketamine enantiomers in MCTA was not accomplished. Thus, in this study a MCTA column was used for enantiomeric separation of anesthetic ketamine (free base). The effect of temperature on chromatographic separation parameters was evaluated at 303, 313, and 323 K. Moment analysis was used to obtain the total porosity, bed porosity, equilibrium constants, axial dispersion, and mass-transfer coefficients.

THEORY

Moment Analysis and Plate Height Equation

The hydrodynamics of a chromatographic column can be described by the analysis of the residence-time distribution of the eluent. Moment analysis is the usual tool for the determination of axial dispersion, equilibrium, and mass transfer parameters from pulse experiments. This technique consists of analyzing the solute concentration as a function of time at the outlet of a fixed bed in response to the solute concentration pulse at the entrance of the bed (22, 23).

The first absolute moment μ is related to the peak retention time, and therefore to the strength of binding (i.e., with the equilibrium constant). The second central moment is related to the band broadening, caused by departures form equilibrium. When the exiting peak is Gaussian, the second moment is equal to the variance σ^2. The first and second moments are expressed as follows (24, 25):

$$\mu = \frac{\int_0^\infty c(t, z = L) t dt}{\int_0^\infty c(t, z = L) dt} \tag{1}$$

$$\sigma^2 = \frac{\int_0^\infty c(t, z = L)(t - \mu)^2 dt}{\int_0^\infty c(t, z = L) dt} \tag{2}$$

Thus, the first and second moment can be analyzed by Eqs. (3) and (4) derived from Eqs. (1) and (2) as:

$$\mu = \frac{L}{u}\left[1 + \left(\frac{1-\varepsilon}{\varepsilon}\right)K\right] + \frac{t_p}{2} \tag{3}$$

$$\sigma^2 = \frac{2L}{u}\left\{\frac{D_L}{u^2}\left[1 + \left(\frac{1-\varepsilon}{\varepsilon}\right)K\right]^2 + \left(\frac{1-\varepsilon}{\varepsilon}\right)\frac{K}{k_m}\right\} + \frac{t_p^2}{12} \tag{4}$$

where

$$K = \varepsilon_p + (1 - \varepsilon_p)K_p \tag{5}$$

In Eqs. (3) and (4), L is the column length, u the superficial velocity of fluid phase, ε the bed porosity, ε_p the particle porosity, K_p the equilibrium adsorption constant, t_p the injection time, D_L the axial dispersion coefficient, and k_m is the overall mass-transfer coefficient.

From the moment analysis of the solution of the general rate model, in the Lapalce domain, the expression for the height equivalent to a theoretical plate (HETP) was calculated as follows (25):

$$\text{HETP} = \frac{\sigma^2}{\mu^2}L = 2\frac{D_L}{u} + 2u\left(\frac{\varepsilon}{1-\varepsilon}\right)\frac{1}{Kk_m}\left(1 + \left(\frac{\varepsilon}{1-\varepsilon}\right)\frac{1}{K}\right)^{-2} \quad (6)$$

Equation (6) contains two separate parameters of interest, the axial dispersion coefficient and overall mass-transfer coefficient. It is evident from the equation that the contribution of axial dispersion and the various mass-transfer resistances are linearly additive (26).

Axial Dispersion Coefficient

When a fluid flows through a packed bed, there is a tendency for axial mixing to occur, contributing to the band broadening and reducing the efficiency of separation. All the phenomena contributed to axial mixing, except that the mass-transfer resistance, are lumped into an axial dispersion coefficient. It is usually assumed that D_L is the combined result of two different mechanisms, molecular diffusion and eddy diffusion. In a packed bed, it is impossible for the mobile phase to move very far along a straight line without hitting the surface particle. The channels follow tortuous paths around the particles. As a first approximation, molecular diffusion and eddy diffusion are additive, and D_L is given by

$$D_L = \gamma_1 D_m + \gamma_2 d_p u \quad (7)$$

where D_m is the molecular diffusion, γ_1 and γ_2 are geometrical constants, and d_p the particle diameter (25). For enantioseparation of chiral substances whose physical properties (including diffusion coefficients D_m) are identical, their axial dispersion coefficients D_L are equal (26).

D_L can also be expressed as $D_L = \tau D_m + \lambda u$ for convenience, where τ is the tortuosity factor for a packed bed column and λ the flow-geometry dependent constant. In a liquid system, the molecular diffusion of the liquid is too small to contribute significantly to axial dispersion, even at low Reynolds numbers (26). Therefore, the molecular diffusion can be neglected and Eq. (7) can be simplified as:

$$D_L = \lambda u \quad (8)$$

Correlations for Mass Transfer Parameters

The overall mass-transfer resistance ($1/k_m$) is composed of two separate mass-transfer mechanisms—the external and the internal resistances to mass transfer (27):

$$\frac{1}{k_m} = \frac{d_p}{6k_f} + \frac{d_p^2}{60\varepsilon_p D_p} \tag{9}$$

where k_f is the external film mass transfer coefficient and D_p is the pore diffusion coefficient. The Wilson-Geankoplis equation can be used to estimate k_f. This equation is valid for liquid system in which $0.0015 < \mathrm{Re}_p < 55$

$$Sh \equiv \frac{d_p k_f}{D_m} = \frac{1.09}{\varepsilon}(Sc)^{1/3}(\mathrm{Re})^{1/3} \tag{10}$$

where Sh, Sc and Re are dimensional Sherwood, Schmidt, and Reynolds numbers, and D_m is the molecular diffusion. The value of D_m can be estimate by the Wilke-Chang equation

$$D_m = 7.4 \cdot 10^{-8} \frac{(\phi M)^{1/2} T}{\eta V_b^{0,6}} \tag{11}$$

where ϕ denote the association coefficient (it takes account of the molecular interactions of solute-solvent due to hydrogen binding), M is the molecular mass, η the viscosity, T the absolute temperature, and V_b is the molar volume at normal boiling point (6).

EXPERIMENTAL SECTION

Material and Equipments

Racemic and pure enantiomers of Ketamine (free base) were furnished by Cristália Pharmaceutical Company (Itapira-SP, Brazil). The mobile phase used in this work was ethanol HPLC-grade (J. T. Baker), in which ketamine is easily dissolved. MCTA offers versatility and low cost, when compared to other CSPs, and was purchased from Macherey–Nagel. The adsorbent particles have 15–25 μm of particle diameters. The semi-preparative stainless steel column (20 × 0.77 cm ID) was packed with adsorbent, employing methanol as solvent. Before packing, the swelling of MCTA was carried out by boiling in ethanol for about 30 min. 1,3,5, tri-*tert*-butylbenzene (TTBB) was purchased from Aldrich. TTTB and the pure enantiomers (*R* and *S*) were dissolved separately in ethanol. These solutions were previously degasified in a COLE PARMER 8892 ultrasonic bath.

The chromatographic experiments were performed in a HPLC system (WATERS 125) equipped with a UV detector (WATERS 2487), temperature

controller, two pumps, and a digital data acquisition system. The signal was monitored by the UV detector with a wavelength of 254 nm.

Experimental Procedures

All chromatograms were obtained under isocratic conditions with ethanol as a mobile phase. The hold-up volume was measured and corrected for the dead volume contribution of the liquid chromatography, by replacing the column with a zero-volume connector. The experiments were performed at different mobile phase flow-rates (0.2, 0.4, 0.6, 0.8, and 1.0 mL/min) and temperatures (303, 313 e, 323 K). Small pulses (20 μL) of dilute solutions were injected into the column after a time interval necessary for the stabilization of the system. The chromatographic data were analyzed by moment method.

RESULTS AND DISCUSSION

Effect of Temperature on Elution Profiles and Retention Data

Figure 3 shows the elution profile of ketamine enantiomers at 303, 313, and 323 K and flow-rate at 1.0 mL/min. The first peak observed in Fig. 3 can be attributed to a small impurity of racemic ketamine. As expected result, the retention times decrease with increasing column temperature. A significant improvement in the elution profiles was observed while increasing the temperature from 303 to 323 K. For both enantiomers the band widths decrease

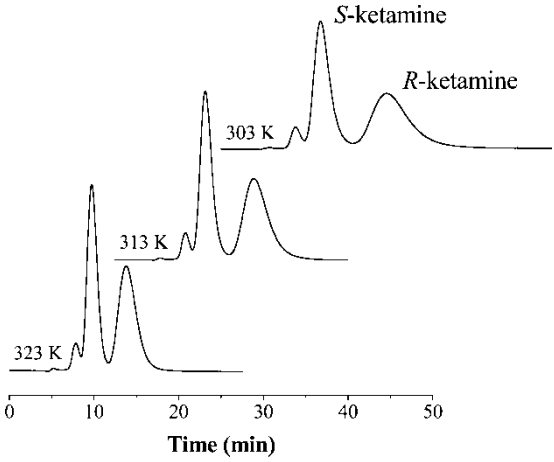

Figure 3. Effect of temperature on the retention time in the enantiomeric separation of ketamine at 303, 313, and 323 K. Experimental conditions: Flow-rate at 1.0 mL/min; Injection volume 20 μL; Wavelength $\lambda = 254$ nm.

Table 1. Capacity factors (k') and selectivity (α) of ketamine enantiomers at 1.0 mL/min

Temperature (K)	$k'_{S\text{-ketamine}}$	$k'_{R\text{-ketamine}}$	α
303	0.90	2.18	2.41
313	0.73	1.65	2.23
323	0.60	1.25	2.07

$[k' = (t_R - t_0)/t_0]$.
$[\alpha = k'_{S\text{-ketamine}}/k'_{R\text{-ketamine}}]$.

sharply. However, the more retained enantiomer (*R*-ketamine) demonstrated larger band broadening than the less retained enantiomer (*S*-ketamine). A similar behavior was reported by Jacobson et al. (9) in the chromatographic enantioseparation of Tröger's base on MCTA under linear conditions. The authors reported that this is due to a combination of a decrease in their retention times and an increase in the column efficiency with increasing temperature.

The system presented good performance separation. As shown in Table 1 the selectivity (α) and the capacity factors (k') decreased with increasing temperature. However, α values were higher than 2. Okamoto and Kaida (10) reported that in most separations with polysaccharide phases, complete separation of enantiomers is attained if selecitivity is larger than 1.2. As shown in Fig. 4, the changes of α of ketamine enantiomers are nearly the same with the flow-rate of the mobile phase.

In most cases, selectivity and resolution of the enantiomers decrease with an increase in temperature. However, α does not adequately describe the separation of enantiomers, since it does not include information about peak widths (28). Resolution (R_S) is given by the relationship between the

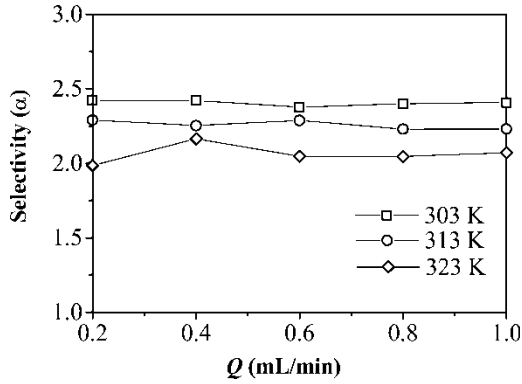

Figure 4. Changes of selectivity with mobile phase flow-rate at (□) 303 K, (○) 313 K, and (◇) 323 K.

difference of retention time of each enantiomer and the bandwidth (w_b) of each elution peak, according to the following equation:

$$R_S = 2\frac{(t_{R,2} - t_{R,1})}{(w_{b,1} + w_{b,2})} \tag{12}$$

Figure 5 shows that the resolution is strongly influenced by the column temperature. The resolution decreases with an increase in the temperature. Since the binding energy decreases with an increase in the temperature, the retention time decreases, the enantiomeric molecules could not interact with stationary phase and the resolution decrease. It was also found that the flow-rate of mobile phase affects the resolution. An increase in the flow-rate causes a decrease in the resolution due to a decrease in the difference between the retention times of each enantiomer.

Measurement of the Total and Bed Porosities

Three different types of column porosity, which are total porosity (ε_T), external porosity or bed porosity (ε), and internal porosity or particle porosity (ε_p), are related by equation (26):

$$\varepsilon_T = \varepsilon + (1 - \varepsilon)\varepsilon_p \tag{13}$$

The total porosity was measured by the pulse-response experiments of non-adsorbed component TTBB to the stationary phase. This component enters the pore system but does not adsorb on the surface of the stationary phase, the retention time of such a component is given by the mean residence time (t_{0R}), as:

$$\mu \text{ (or } t_{0R}) = \frac{L}{u}\varepsilon_T = \frac{L}{u}[\varepsilon + (1 - \varepsilon)\varepsilon_p] \tag{14}$$

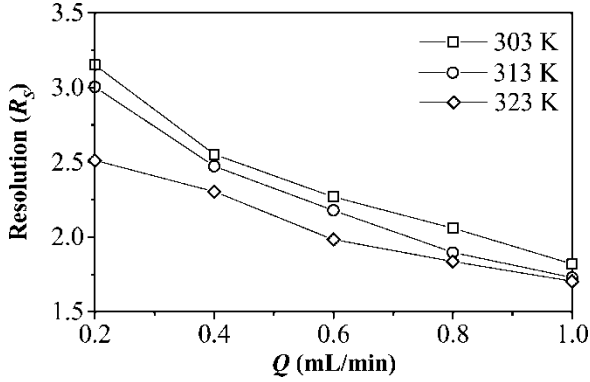

Figure 5. Variation of the resolution of ketamine enantiomers with mobile phase flow-rate at (□) 303 K, (○) 313 K, and (◇) 323 K.

The bed porosity was measured in a similar manner by the pulse experiments of a nonadsorbed blue dextran, as the procedure described by Silva Jr. et al. (21). This component is sufficiently large and does not penetrate the pores of MCTA particles in elution. In this case, the bed porosity can be calculated by the mean residence as follows:

$$\mu \text{ (or } t_{0R}) = \frac{L}{u}\varepsilon \tag{15}$$

In this work, the porosities values did not have significant variation with temperature. From the plot of mean retention time vs. the inverse of superficial velocity (L/u) (not shown), the total porosity measured was 0.66 and bed porosity measured was 0.39. The value of particle porosity was estimated by Eq. (13) and found to be 0.45. The literature presents values of total porosity for columns packed with MCTA and using ethanol as eluent ranging from 0.60 up to 0.71 (6, 7, 9, 15, 29). A total porosity of 0.67 with bed and particle porosity of 0.40 and 0.45, respectively (using methanol as eluent), were reported (13). The values of porosities measured in the present work are inside the range reported in the literature.

Measurement of Equilibrium Adsorption Data

A previous study was performed to obtain the nonlinear adsorption isotherms of ketamine enantiomers on MCTA (21). Based on that study, we used dilute solutions in this work to warrant the linearity of the adsorption isotherms.

The linear equilibrium constants for both enantiomers of ketamine were determined by first moment plots (Fig. 6). All fitted lines were in good agreement with the experimental points. According to Eq. (3), the equilibrium constants were determined from the slopes of the straight lines and the results are presented in the Table 2. Obviously, the change in temperature influences differently the interaction of the ketamine enantiomers with MCTA. The equilibrium constants were found to be greater than unity decrease with increasing temperature. From these results we can concluded that there are strong interactions between both enantiomers and the chiral column. The column has a grater affinity for *R*-ketamine than for *S*-ketamine. This may be explained by different steric interactions between each enantiomer and the chiral column.

Standard thermodynamic functions K_p, ΔG, ΔH, and ΔS at infinite dilution can be determined from the slope of the initial tangent of the isotherm (linear isotherm) (30). Since the molar Gibbs free energy (ΔG) of the adsorption process is related to the equilibrium constant, the entropy change and the heat of adsorption at constant temperature then

$$\Delta G = -RT \ln K_p = \Delta H - T\Delta S \tag{16}$$

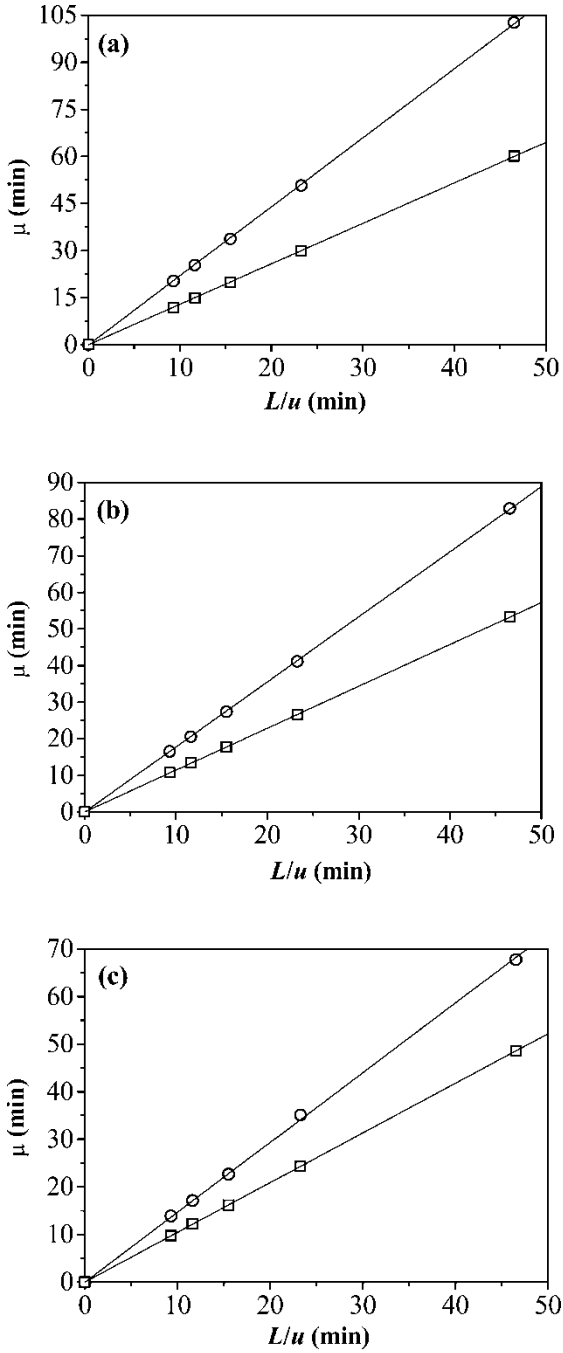

Figure 6. Plot of the first moment *vs.* the inverse of superficial velocity of *R*-ketamine (○) and *S*-ketamine (□) at (a) 303 K, (b) 313 K, and (c) 323 K.

Table 2. Equilibrium adsorption constants (K_p), entropy change (ΔS) and heat of adsorption (ΔH) of ketamine enantiomers

Temperature (K)	K_p *S*-ketamine	K_p *R*-ketamine
303	1.85	4.51
313	1.42	3.28
323	1.13	2.37
ΔS	−63.13 J/mol	−73.79 J/mol
ΔH	−20.07 kJ/mol	−26.16 kJ/mol

where R is the gas constant, T is the solution temperature, and ΔS and ΔH are the entropy change and heat of adsorption, respectively. Rearranging Eq. (16), the equilibrium adsorption constant thus varies with the temperature according to the following equation:

$$\ln K_p = \frac{\Delta S}{R} - \frac{\Delta H}{RT} \tag{17}$$

When the measurement of thermodynamic parameters showed that ΔH and ΔS have the same negative sign, this means that there is an enantioselective temperature (T_{iso}) for these enantiomers. According to Eq. (18), we get the following relationship at values of $\alpha = 1$:

$$T_{iso} = \frac{\Delta H}{\Delta S} \tag{18}$$

At T_{iso} no separation of enantiomers will occur. At temperatures higher than T_{iso}, the enantiomer elution order should be reversed. However, for most enantiomers, T_{iso} is much higher than the working temperature range (31). In this work, a linear dependence of natural logarithms ($\ln K_p$) vs. inverse of temperature ($1/T$) was observed for both enantiomers (Fig. 7). The entropy change and heat of adsorption calculated from the intercept and the slopes of the straight line in Fig. 7 are presented in Table 2. The measurement of thermodynamic parameters showed that ΔH and ΔS have the same negative sign and the T_{iso} was found to be 346 K.

Measurement of the Axial Dispersion Coefficients and Mass-Transfer Parameters

Combining Eqs. (6), (8), and (9) and rearranging,

$$\mathrm{HETP} = 2\lambda + 2u\left(\frac{\varepsilon}{1-\varepsilon}\right)\left(\frac{d_p}{6\,k_f} + \frac{d_p^2}{60\varepsilon_p D_p}\right)\left(1 + \left(\frac{\varepsilon}{1-\varepsilon}\right)\frac{1}{K}\right)^{-2} \tag{19}$$

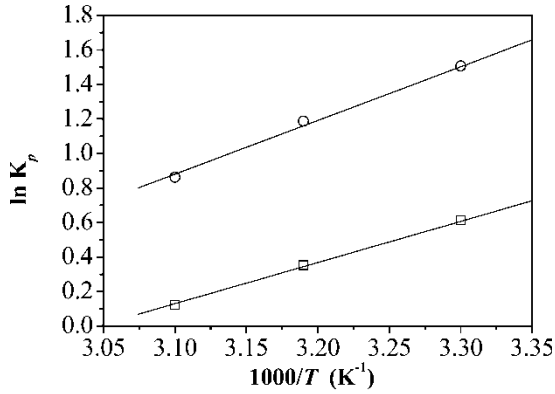

Figure 7. Temperature dependence of the equilibrium adsorption constant of *R*-ketamine (○) and *S*-ketamine (□).

The external mass-transfer coefficient, which is flow-rate dependent, was obtained from Eq. (10). So, isolating the term related to the external resistance to the mass transfer on the right-hand side in Eq. (19):

$$\mathrm{HETP_{mod}} = 2\lambda + 2u\left(\frac{\varepsilon}{1-\varepsilon}\right)\left(\frac{d_p^2}{60\varepsilon_p D_p}\right)\left(1+\left(\frac{\varepsilon}{1-\varepsilon}\right)\frac{1}{K}\right)^{-2} \qquad (20)$$

where

$$\mathrm{HETP_{mod}} = \mathrm{HETP} - 2u\left(\frac{\varepsilon}{1-\varepsilon}\right)\left(\frac{d_p}{6k_f}\right)\left(1+\left(\frac{\varepsilon}{1-\varepsilon}\right)\frac{1}{K}\right)^{-2} \qquad (21)$$

Figures 8–10 show the variation of the column efficiency for each compound at 303, 313, and 323 K. As expected, the efficiency of the

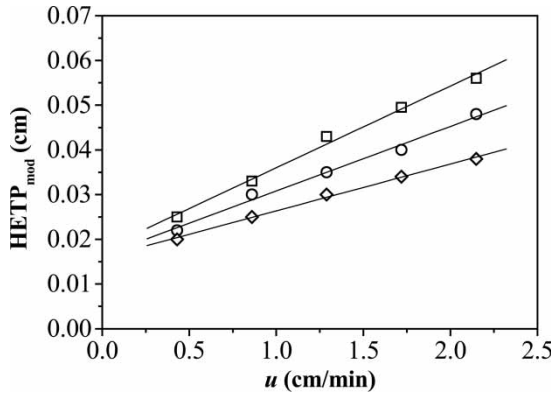

Figure 8. $\mathrm{HETP_{mod}}$ plot for TTBB at (□) 303 K, (○) 313 K, and (◇) 323 K.

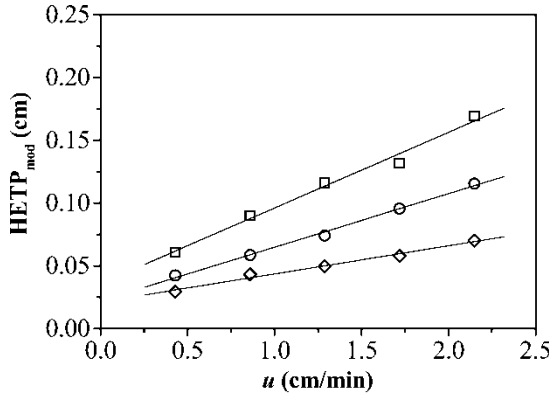

Figure 9. $HETP_{mod}$ plot for *S*-ketamine at (□) 303 K, (○) 313 K, and (◇) 323 K.

column increases with the increase in temperature. For all temperatures, the more retained enantiomer (*R*-ketamine) had the lowest efficiency, followed by the less-retained enantiomer (*S*-ketamine), and finally TTBB, with the highest efficiency.

In the $HETP_{mod}$ plot of the non-retained compound TTBB (Fig. 8), which is considered not adsorbed in the chiral stationary phase, mass-transfer resistance can be neglected and $HETP_{mod}$ is considered to be independent of the interstitial velocity of mobile phase (u). A straight line with very little variation with the flow-rate was observed. This means that the axial dispersion for TTBB is dominant in the chiral column. For both enantiomers of ketamine the $HETP_{mod}$ plot failed to show a minimum (Figs. 9 and 10). This result indicates that the effects of axial dispersion and mass-transfer resistance control the efficiency of the column. The influence of the molecular

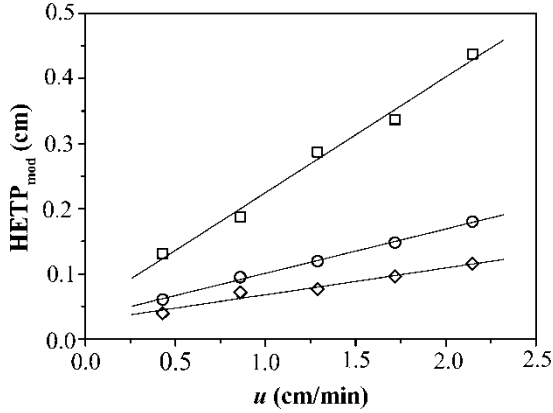

Figure 10. $HETP_{mod}$ plot for *R*-ketamine at (□) 303 K, (○) 313 K, and (◇) 323 K.

Table 3. Axial dispersion (D_L) and pore diffusion coefficients (D_p) of TTBB and ketamine enantiomers obtained from the $HETP_{mod}$ plots

Temperature (K)	TTBB	$D_L \cdot 10^2$ (cm)		$D_p \cdot 10^6$ (cm^2/min)	
		S-ketamine	*R*-ketamine	*S*-ketamine	*R*-ketamine
303	0.89	1.80	1.90	1.10	0.32
313	0.82	1.11	1.64	1.66	0.78
323	0.80	1.06	1.35	3.39	1.48

diffusion on the HETP is significant only for low feed flow-rates. Therefore, we concluded that it was reasonable to disregard the term that refers to molecular diffusion for the axial dispersion. The slopes of both lines of each enantiomer in these plots were relatively high, which means that the mass-transfer resistance of each enantiomer inside the MCTA particles is therefore high.

The mass-transfer parameters are shown in Table 3. Pore diffusion and axial dispersion coefficients were obtained from the slope and intercept of straight lines in the $HETP_{mod}$ plots, according to Eq. (20). The result shows that the axial dispersion coefficients were found to be approximately the same order of magnitude. However, we observe that it decreases with increasing temperature. Jacobson et al. (9) reported that this can be attributed to the particle size distribution of the packing material, and to its irregularity. Table 3 shows that pore diffusion coefficients for both enantiomers increase with increase in the temperature. According to the magnitude of external mass-transfer coefficients, we concluded that the internal resistance to the mass-transfer controls the mass-transfer process in this chiral column because $d_p/6kf <<< d_p^2 / 60\varepsilon_p D_p$, as reported by Miyabe and Guiochon (6) and Jacobson et al. (9), the main contribution to the band broadening in a MCTA column is low mass transfer kinetics. In fact, under linear conditions the elution profiles of racemic ketamine (Fig. 3) presented a large retention time and a strong band broadening, mainly for the more retained enantiomer. These phenomena can be attributed to a slow pore diffusion coefficient of ketamine enantiomers in this CSP. Since an increase in temperature decreases the retention time, the band broadening is also reduced. This behavior is attributed to the more favorable kinetics of mass transfer with increase of the pore diffusion coefficients.

CONCLUSIONS

In this study, the effect of temperature on the kinetic and equilibrium constants of chromatographic separation of ketamine enantiomers in MCTA was evaluated by moment analysis. The equilibrium constants decrease with

temperature rise and the chiral stationary phase exhibits a higher affinity for the *R*-ketamine than for *S*-ketamine. The axial dispersion coefficients present values of the same order of magnitude. The pore diffusion coefficients increase with increase in temperature. A larger band broadening was observed. However, a significant improvement in the elution profiles was obtained with temperature increase. This phenomenon can be attributed to an increase in the pore diffusion coefficients. We concluded that the contribution of pore diffusion to band broadening is more important than axial dispersion, external film mass transfer and equilibrium adsorption. Based on the presented results, a better understanding of the mass-transfer processes and equilibrium behavior of ketamine enantiomers in MCTA were obtained. The data obtained in the present work may be employed in computational simulation to predict the separation performance of SMB unity.

NOMENCLATURE

c	Detector response in Eqs. (1) and (2)
d_p	Particle diameter (cm)
D_L	Axial dispersion coefficient ($cm^2 \cdot min^{-1}$)
D_m	Molecular diffusivity ($cm^2 \cdot min^{-1}$)
HETP	Height equivalent theoretical plate (cm)
k'	Capacity factor
k_m	Overall mass-transfer coefficient (min^{-1})
K	Equilibrium constant in Eq. (5)
K_p	Equilibrium adsorption constant
L	Column length (cm)
M	Molecular mass ($g \cdot gmol^{-1}$)
N_p	Theoretical plate number
R	Universal gas constant ($J \cdot mol^{-1} \cdot K^{-1}$)
T	Temperature (K)
t	Time (min)
t_0	Injection time (min)
t_{0R}	Mean residence time (min)
u	Superficial velocity of fluid phase ($cm \cdot min^{-1}$)
V_b	Molar volume at boiling temperature ($cm^3\ gmol^{-1}$)

Greek Symbols

α	Selectivity
ε	Bed porosity
ε_T	Total column porosity
ε_p	Particle porosity
μ	First moment (min)

σ^2	Second moment (min^2)
ϕ	Association coefficient
η	Viscosity (cP)
τ	Tortuosity
λ	Flow-geometry constant

ACKNOWLEDGMENTS

The authors are greateful to FINEP (Proc. No. 77.97.0503.00), CNPq (Proc. No. 465707/200-9), and FAPESP (Proc. 01/13168-0) for financial support and to the CRISTÁLIA Pharmaceutical Company, for kindly providing the racemic anesthetic ketamine and its standard pure enantiomers.

REFERENCES

1. Seidel-Morgenstern, A. (2004) Experimental determination of single solute and competitive adsorption isotherms. *J. Chromatogr. A*, 1037: 255.
2. Lai, S.-M and Lin, Z.-C. (1999) Measurement of adsorption characteristics of enantiomers on chiral columns: Comparison of the frontal and elution chromatographic techniques. *Sep. Sci. Technol.*, 34: 3173–3196.
3. Schulte, M., Ditz, R., Devant, R.M., Kinkel, J.N., and Charton, F. (1997) Comparison of the specific productivity of different chiral stationary phases used for simulated moving-bed chromatography. *J. Chromatogr. A*, 769: 93.
4. Miyabe, K. and Guiochon, G. (2000) A study of mass transfer kinetics in an enantiomeric separation system using a polymeric imprinted stationary phase. *Biotechnol. Prog.*, 16: 617.
5. Wankat, P.C. (1994) *Rate-Controlled Separations*; Chapman & Hall: London.
6. Miyabe, K. and Guiochon, G. (1999) Kinetic study of the mass transfer of *S*-Tröger base in the system cellulose triacetate and ethanol. *J. Chromatogr. A*, 849: 445.
7. Seidel-Morgenstern, A. and Guiochon, G. (1993) Modelling of the competitive isotherms and the chromatographic separation of two enantiomers. *Chem. Eng. Sci.*, 48: 2787.
8. Okamoto, Y., Kawashima, M., Yamamoto, K., and Hatada, K. (1984) Useful chiral packing materials for high-performance liquid chromatography resolution: Cellulose triacetate and tribenzoate coated on macroporous silica gel. *Chem. Let.*, 739.
9. Jacobson, C.S., Seidel-Morgenstern, A., and Guiochon, G. (1993) Study of band broadening in enantioselective separations using microcrystalline cellulose triacetate: I. The linear case. *J. Chromatogr.*, 637: 13.
10. Okamoto, Y. and Kaida, Y. (1994) Resolution by high-performance liquid chromatography using polysaccharide carbamates and benzoates as chiral stationary phases. *J. Chromatogr. A*, 666: 565.
11. Hasse, G. and Hagel, R. (1973) A complete separation of a racemic mixture by elution chromatography on cellulose triacetate. *Chromatographia*, 6: 277.
12. Pirkle, W.H. and Pochapsky, T.C. (1989) Considerations of chiral recognition relevant to the liquid chromatographic separation of enantiomers. *Chem. Rev.*, 89: 347.

13. Pais, S.L., Loureiro, J.M., and Rodrigues, A.E. (1998) Separation of enantiomers of a chiral epoxide by simulated moving bed chromatography. *J. Chromatogr. A*, 827: 215.
14. Rizzi, A.M. (1989) Evaluation of the optimization potential in high-performance liquid chromatographic separations of optical isomers with swollen microcrystalline cellulose triacetate. *J. Chromatogr.*, 478: 1001.
15. Rizzi, A.M. (1989) Band broadening in high performance liquid chromatographic separations of enantiomers with swollen microcrystalline cellulose triacetate packings: Influence of capacity factor, analyte structure, flow velocity and columns loading. *J. Chromatogr.*, 478: 71.
16. Rizzi, A.M. (1989) Band broadening in high performance liquid chromatographic separations of enantiomers with swollen microcrystalline cellulose triacetate packings: Influence of eluent composistion, temperature and pressure. *J. Chromatogr.*, 478: 87.
17. Yanagihara, Y., Ohtani, M., Kariya, S., Uchino, K., Aoyama, T., Yamamura, Y., and Iga, T. (2000) Stereoselective high-performance liquid chromatographic determination of ketamine and its active metabolic, norketamine, in humam plasm. *J. Chromatogr. B*, 746: 227.
18. Svensson, J. and Gustafsson, L.L. (1996) Determination of ketamine and norketamine enantiomers in plasma by solid-phase extraction and high-performance liquid chromatography. *J. Chromatogr. B*, 678: 373.
19. Nishizawa, N., Nakao, S., Nagata, A., Hirose, T., Masuzawa, M., and Shingu, K. (2000) The effect of ketamine isomers on both mice behavioral responses and c-Fos expression in the posterior cingulate and retrosplenial córtices. *Brain Res.*, 857: 188.
20. Santos, M.A.G., Veredas, V., Silva, I.J., Jr., Correia, C.R.D., Furlan, L.T., and Santana, C.C. (2004) Simulated moving bed adsorption for separation of racemic mixtures. *Braz. J. Chem. Eng.*, 21: 127.
21. Silva, I.J., Jr., Santos, M.A.G., Veredas, V., and Santana, C.C. (2005) Experimental determination of chromatographic separation parameters of ketamine enantiomers on MCTA. *Sep. Purif. Technol.*, 43: 103–110.
22. Duan, G., Ching, C.-B., and Swarup, S. (1998) Kinetic and equilibrium study of the separation of propranolol enantiomers by high performance liquid chromatography on a chiral adsorbent. *Chem. Eng. J.*, 69: 111–117.
23. Miyabe, K. and Suzuki, M. (1992) Chromatography of liquid-phase adsorption on octadecylsilyl-silica gel. *AIChE J.*, 38 (6): 901–909.
24. Guiochon, G., Shirazi, S.G., and Katti, A.M. (1994) *Fundamentals of Preparative and Nonlinear Chromatography*; Academic Press: Boston.
25. Ruthven, D.M. (1984) *Principles of Adsorption and Adsorption Process*; Wiley: New York.
26. Wang, X. and Ching, C.-B. (2002) Kinetic and equilibrium study of the separation of three chiral center drug, nadolol, by HPLC on a novel perphenyl carbamoylated β-cyclodextrin bonded chiral stationary phase. *Sep. Sci. Technol.*, 37: 2567.
27. Ma, Z. and Wang, N.-H.L. (1997) Standing wave analysis of SMB chromatography: Linear systems. *AIChE J.*, 43: 2488.
28. Rojkovičová, T., Lehotay, J., Krupčík, J., Fedurcová, A., Čižmárik, J., and Armstrong, D.W. (2004) Study of the mechanism of enantioseparation: VII. Effect of temperature on retention of some enantiomers of phenylcabamic acid derivates on a teicoplanin aglycone chiral stationary phase. *J. Liquid. Chromatogr. Relat. Technol.*, 11: 1563–1670.

29. Rearden, P., Sajonz, P., and Guiochon, G. (1998) Detailed study of the mass transfer kinetics of tröger base on cellulose triacetate. *J. Chromatogr. A*, 813: 1.
30. Seidel-Morgenstern, A. and Guiochon, G. (1993) Thermodynamics of the adsorption of Tröger's base enantiomers from ethanol on cellulose triacetate. *J. Chromatogr.*, 631: 37.
31. Ahuja, S. (2000) *Chiral Separations by Chromatography*; Oxoford University Press: New York.